

Inverse Source of Circumference Geometries: SVD Investigation Based on Fourier Analysis

Giovanni Leone^{*}, Maria A. Maisto, and Rocco Pierri

Abstract—The role of the source geometry is investigated within the realm of inverse source problems. In order to examine the properties of the far zone radiation operator of some 2D curved sources its Singular Value Decomposition (SVD) is studied, either analytically, when possible, or numerically. This allows to evaluate the number of independent pieces of information, i.e., the number of degrees of freedom (NDF), of the source and to point out the set of far zone fields corresponding to stable solutions of the inverse problem. In particular, upper bounds for the NDF are obtained by exploiting Fourier series representations of the singular functions. Both curved (i.e., circumference and arc of circumference) and rectilinear geometries are considered, pointing out the role of limited angular observation domains. Moreover, in order to obtain some clues about the resolution achievable in the inverse source problem, a point-spread function analysis is performed. The latter reveals a spatially variant resolution for limited angular observation domains. The practical relevance of these results is highlighted with numerical examples of array diagnostics.

1. INTRODUCTION

SHAPED, i.e., not rectilinear or planar, sources find increasing applications in both radar surveillance and wireless communication. In fact, the latitude provided by the geometry makes it possible to achieve better performances, for instance, when hemispherical coverage is required [1]. In addition, a conformal array can radiate identical focusing beams pointing at different directions. At the same time, it may allow a uniform coverage within larger angular sectors. In MIMO communications, the number of independent SISO channels depends on the sources' and receivers' configurations.

In any case, it is of interest to properly design the antenna system to achieve the best radiating performances. However, most synthesis procedures are tailored to rectilinear or planar sources, so that often a brute force approach based on numerical optimization [2] of source parameters is adopted for different geometries. Therefore, it would prove very useful to investigate an approach capable of relating the expected performances to the source geometry before entering the synthesis procedure.

At the same time, for antenna testing and diagnostics [3], the knowledge of the minimum number of independent pieces of 'information' about the radiated field allows to drastically reduce measurement time. This, in turn, is connected to the source geometry. In any case, attention can be focused on dependence between the source geometry and the mathematical properties of the radiation operator, relating the source current to its radiated field. To accomplish such a task the singular value decomposition (SVD) of the involved operator is a natural and fundamental tool. Indeed, the SVD allows the evaluation of the so-called number of degrees of freedom (NDF) [4]. In turn, this is strongly connected both to the set of source current that can be stably retrieved against the noise [5] in diagnostics problems and to the set of radiation patterns that the source is able to radiate. Indeed, such sets are spanned by certain subsets of singular functions depending on the noise, the a priori constraints about

Received 21 June 2018, Accepted 26 October 2018, Scheduled 20 December 2018

^{*} Corresponding author: Giovanni Leone (giovanni.leone@unicampania.it).

The authors are with the Dipartimento di Ingegneria, Università della Campania Luigi Vanvitelli, via Roma 29, Aversa I-81031, Italy.

the unknown and data spaces, and so on. Compactness [6] of the involved operators is the relevant mathematical property connected to this point since the corresponding singular values (SVs) decay to zero as their index increases. This affects the inverse source problem thus makes it severely ill-posed. In order to obtain stable reconstructions, the problem must be regularized, so that approximate solutions arise as a result of a trade-off between stability and accuracy [7]. This strongly limits the NDF and, hence, the resolution achievable in inverse source problems. In order to quantify the ‘resolution power’ of the imaging procedure, i.e., the ability to distinguish two close point-like sources, the point-spread function (PSF) is usually considered. It is defined as the reconstruction of an impulsive source and the width of its main lobe provides a measure of the resolution. It can be proved that the PSF can be expressed in terms of the NDF and the singular functions [8]. The behavior of the SVs plays an important role in achieving a stable solution to any inverse problem, when the simplest regularization scheme, the truncated singular value decomposition (TSVD), is adopted [7]. Accordingly, the NDF can be estimated as the number of SVs greater than a threshold dictated by the noise. When the SVs exhibit a step-like behavior, the truncation index for the regularized inversion can be defined regardless of the noise level. On the contrary, when the latter does not occur, the truncation index of the TSVD procedure may be dependent on data uncertainties.

Inspired by [8–13], the aim of this paper is to investigate the role of some 2D scalar source geometries in the SVD of the relevant far zone radiation operator. Since it is not always known in closed form, sometimes, information about the SVD can be gained by considering different representations of the pertinent singular functions, such as the Fourier series. In [12] a similar analysis is performed for arc sources observed over a circumference. Here a more general situation where both observation domain and the source are circumference arcs is considered. Moreover, the case of a linear source is addressed.

First, in Section 2, some results obtained in [12] about the circumference source are recalled. Next, we deal with a geometry where both the observation domain and the source are circumference arcs. An asymptotic analysis about the harmonic content of the singular functions, allowing to obtain some information about the SVs behavior, is developed, so as to introduce an upper bound on the NDF. Finally, a linear source is considered. In Section 3, the role of the observation domain in defining the resolution in inversion procedures is pointed out, by theoretical and numerical examination of the relevant PSFs. The results are applied to the localization of point-like sources. Section 5 is devoted to show the practical relevance of the approach by numerical examples of source reconstructions and array diagnostics. The role of the SVD knowledge is appreciated for a reliable prediction of the results.

2. SVD INVESTIGATION

2.1. The Mathematical Approach

Let us consider a 2D scalar z -invariant current source $J(\underline{r})$ supported over a curve c belonging to the x - y plane. The electric field $E(\theta)$ radiated by the source is collected in far zone over $OD = [-\gamma, \gamma]$. At a single frequency $E(\theta)$, apart from some inessential factors, is given by

$$E(\theta) = \int_c J(\underline{r}') e^{j\beta \underline{r}' \cdot \hat{r}(\theta)} dc \quad (1)$$

where $\beta = 2\pi/\lambda$ is the free space wave number, and $\hat{r}(\theta) = (\cos \theta, \sin \theta)$ is the unit vector pointing at the observation direction.

The radiation operator mapping the vector space of current functions into the one of the radiated fields is

$$\mathcal{L} : J \in L_c^2 \rightarrow E \in L_{OD}^2 \quad (2)$$

where J and E are assumed to belong to the set of square integrable functions indicated by $L_{(\cdot)}^2$ supported over c and OD , respectively. Since the operator \mathcal{L} is compact, its SVD can be computed for each source shape. It consists of the triple $\{v_n, \sigma_n, u_n\}$ [7] where u_n is the n -th left singular function, σ_n the n -th SV, and v_n the n -th right singular function. In particular, the $\{u_n\}$ functions provide the set of achievable far zone patterns and the $\{v_n\}$ functions the set of the corresponding source currents.

2.2. Circumference Source

Let us suppose that the current J is supported over a circumference, so that $c = \{(\rho, \phi) : \rho = a, \phi \in (-\pi, \pi)\}$ (Fig. 1 depicts the geometry). Then the relevant operator becomes

$$E(\theta) = \int_{-\pi}^{\pi} J(\phi) e^{j\beta a \cos(\theta-\phi)} a d\phi \tag{3}$$

and $OD = [-\pi, \pi]$. The SVD of Eq. (3) for a circumference source is known analytically and reported in [12]. In particular the SVs are proportional to the Bessel functions $J_l(\beta a)$ of first kind and order l with argument βa . In virtue of the asymptotic behavior of these Bessel functions, the SVs decay exponentially fast for indices larger than $N \cong [\beta a]$ ($[\cdot]$ stands for the integer part). This means that the NDF, i.e., the number of independent pieces of information that can be reconstructed in a stable way, can be estimated as $2N + 1$ at most.

Figure 2 displays the behavior of the SVs, which are the Bessel function with βa argument of different order arranged under descending values. From Fig. 2, it can be appreciated that at $n \approx 2N + 1$

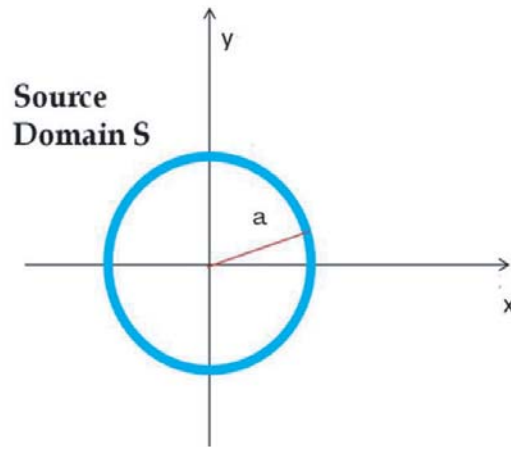


Figure 1. Geometry of a circumference source.

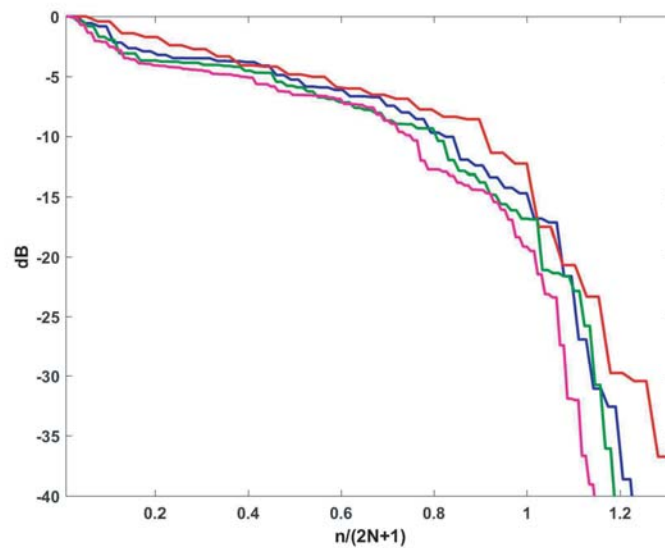


Figure 2. Normalized behavior of the SVs of a circumference source vs. their index normalized to $2N + 1$ for $a = 5\lambda$ (blue line), 3λ (red line), 7λ (green line), 10λ (purple line).

the SVs curve exhibits the knee as predicted, but before it is not flat. Indeed, they vary within an interval as large as 20 dB (the larger the radius, the higher the dynamic). This implies that according to uncertainties affecting the data, the truncation level of the TSVD procedure may occur at indexes n much lower than NDF.

In [12] it is shown that, since the highest values of the Bessel functions are achieved when the order l approaches βa , it can be expected that the first SVs (the more relevant in value) correspond to Bessel function of high order l . Therefore, the application of the TSVD procedure cuts down the lower order ones according to the truncation threshold. Now, since the singular functions $\{v_n\}$ are Fourier harmonics, we can expect that the lower order Fourier harmonics of the source current function may be filtered out by the regularizing imaging algorithm, thus giving rise to a sort of ‘bandpass’ behavior of the reconstruction procedure.

2.3. Limited Observation Domain

Since the space of the far zone fields, defined by the $u_n(\theta)$ functions, is spanned (at most) by $2N + 1$ Fourier harmonics [12], an equivalent set of basis functions is provided by the $2N + 1$ Dirichlet kernels $\frac{\sin[\frac{2N+1}{2}(\theta-\theta_n)]}{\sqrt{2\pi}\sqrt{2N+1}\sin(\frac{\theta-\theta_n}{2})}$ for $\theta_n = \frac{2\pi n}{2N+1}$, and $n = -N, \dots, N$, which are the sampling functions for a periodic function composed of a finite number of Fourier harmonics. This observation allows to associate the degrees of freedom of the source to the samples of the $E(\theta)$ function at $\Delta\theta = \frac{2\pi}{2N+1}$ equispaced angular step.

As a consequence, when the observation domain is reduced to $OD = [-\gamma, \gamma]$ an estimation of the NDF for a circumference source may follow as the number of samples falling within the observation domain, i.e., $2M' + 1$, with $M' \approx N\gamma/\pi$. This, of course, implies that the class of sources that can be reconstructed reduces.

In the following Section further arguments are provided to confirm this result and some consequences highlighted.

2.4. Arc of Circumference

When the conformal curved source becomes a 2α wide arc of circumference (Fig. 3) and $OD = [-\gamma, \gamma]$, the SVD of the relevant operator

$$E(\theta) = \int_{-\alpha}^{\alpha} J(\phi) e^{j\beta a \cos(\theta-\phi)} a d\phi = \mathcal{L}(J) \quad (4)$$

is not known analytically.

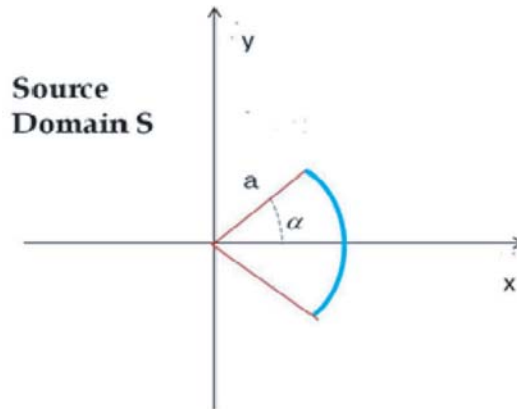


Figure 3. Geometry of a circumference arc source.

Anyway, in order to provide some clues about it and to appreciate the role of the α and γ angles, let us suppose to represent the $v_n(\phi)$ and the $u_n(\theta)$ in terms of Fourier harmonics, that is

$$v_n(\phi) = \sum_{m=-\infty}^{\infty} v_n^m \frac{e^{jm\phi\pi/\alpha}}{\sqrt{2\alpha}} \tag{5}$$

$$u_n(\theta) = \sum_{m'=-\infty}^{\infty} u_n^{m'} \frac{e^{jm'\theta\pi/\gamma}}{\sqrt{2\gamma}} \tag{6}$$

with $\phi \in (-\alpha, \alpha)$ and $\theta \in (-\gamma, \gamma)$ and v_n^m and $u_n^{m'}$ are the respective projections. The singular functions satisfy the coupled singular systems

$$\begin{aligned} \mathcal{L}(v_n) &= \sigma_n u_n \\ \mathcal{L}^\dagger(u_n) &= \sigma_n v_n \end{aligned} \tag{7}$$

where L^\dagger is the adjoint of \mathcal{L} . Consider the first equation of (7)

$$\sum_{m=-\infty}^{\infty} v_n^m \int_{-\alpha}^{\alpha} \frac{e^{jm\phi\pi/\alpha}}{\sqrt{2\alpha}} e^{j\beta a \cos(\theta-\phi)} a d\phi = \sigma_n u_n \tag{8}$$

In order to examine the contribution that each harmonic of v_n provides to u_n , standard stationary phase asymptotic arguments [12] for $\beta a \gg 1$ can be invoked as follows to evaluate Eq. (8).

In fact, the phase function $g(\phi) = \cos(\phi - \theta) + (m\phi\pi)/(\beta a \alpha)$ is stationary when $g'(\phi_0) = -\sin(\theta - \phi_0) + (m\pi)/(\beta a \alpha) = 0$, i.e., $\sin(\theta - \phi_0) = (m\pi)/(\beta a \alpha)$.

A stationary point within the integration interval can occur as long as $(|m|\pi)/(\beta a \alpha) < \eta$ with $\eta = 1$ if $\alpha + \gamma \geq \pi/2$, otherwise $\eta = \sin(\alpha + \gamma)$.

This means that the maximum number of Fourier harmonics necessary to represent $v_n(\phi)$ is $2M + 1$ with $M = \eta\beta a \alpha/\pi$.

Turning now to the second equation of (7) and exploiting the same arguments as before, it can be derived that the maximum number of Fourier harmonics necessary to represent $u_n(\theta)$ is $2M' + 1$ with $M' = \eta\beta a \gamma/\pi$.

This discussion extends that of [12] to finite angular observation domains but does not allow to determine the singular system of \mathcal{L} . However, it can provide interesting clues about it.

Firstly, it allows to define the maximum number of harmonic functions necessary to represent the singular functions for both the current and the radiated field. Accordingly, the NDF may amount to the minimum between $2M + 1$ and $2M' + 1$ at least. Anyway, since the representation basis of the harmonic functions is not the ‘‘extremal’’ one, either $2M + 1$ or $2M' + 1$ provides an upper bound to the NDF.

Moreover, as far as the contribution of an individual harmonic of $v_n(\phi)$ in Eq. (5) to the amplitude of the radiated field is concerned, the higher the harmonic order is, the higher its contribution is on $u_n(\theta)$. This occurs because the amplitude of each Fourier harmonics in Eq. (8) is proportional to $[g''(\phi_0)]^{-1/2}$ (with $g''(\phi_0) = -\cos(\theta - \phi_0) = -\sqrt{1 - [(m\pi)/(\beta a \alpha)]^2}$) by stationary phase arguments so that it is larger for higher order harmonics. Although the Fourier harmonics are not singular functions, this result is in accordance with the above case of the full circumference source, where the higher order singular functions radiate higher fields, and it provides the above mentioned ‘passband’ behavior of the operator again.

The numerical computation of the SVD of Eq. (4) can be accomplished, for instance, by adopting Fourier expansions for both functions as Eqs. (5) and (6) (i.e., $E(\theta) = \sum_l e_l e^{j\theta\pi/\gamma}/\sqrt{2\gamma}$ and $J_S(\phi) = \sum_m \gamma_m e^{jm\phi\pi/\alpha}/\sqrt{2\alpha}$), so that the relevant operator in Eq. (4) can be represented as

$$e_l = 2a\sqrt{\gamma\alpha} \sum_{\nu} j^{\nu} J_{\nu}(\beta a) \text{sinc}(l\pi - \nu\gamma) \sum_m \gamma_m \text{sinc}(m\pi - \nu\alpha) \tag{9}$$

The numerical results confirm the expectations for the present more general case of both finite source and observation domains.

Figures 4 and 5 show the numerically evaluated SVs behavior and singular functions for $a = 3\lambda$, $\alpha = \pi/2$ and $\gamma = \pi/4$. As can be seen while the maximum Fourier estimated harmonic order is $2M + 1 \approx [\beta a] + 1 = 19$, the actual number of the significant SVs before the exponential decay (i.e., the NDF) is 10, lower than the one predicted by the Fourier analysis.

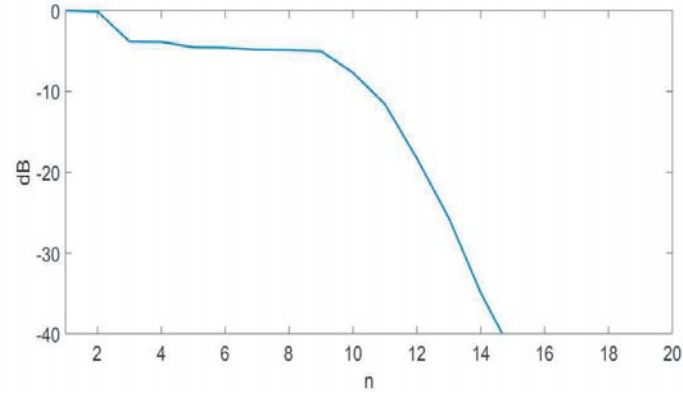


Figure 4. Normalized behavior of the SVs vs their index n for a circumference arc source of radius $a = 3\lambda$, $\alpha = \pi/2$ and $\gamma = \pi/4$.

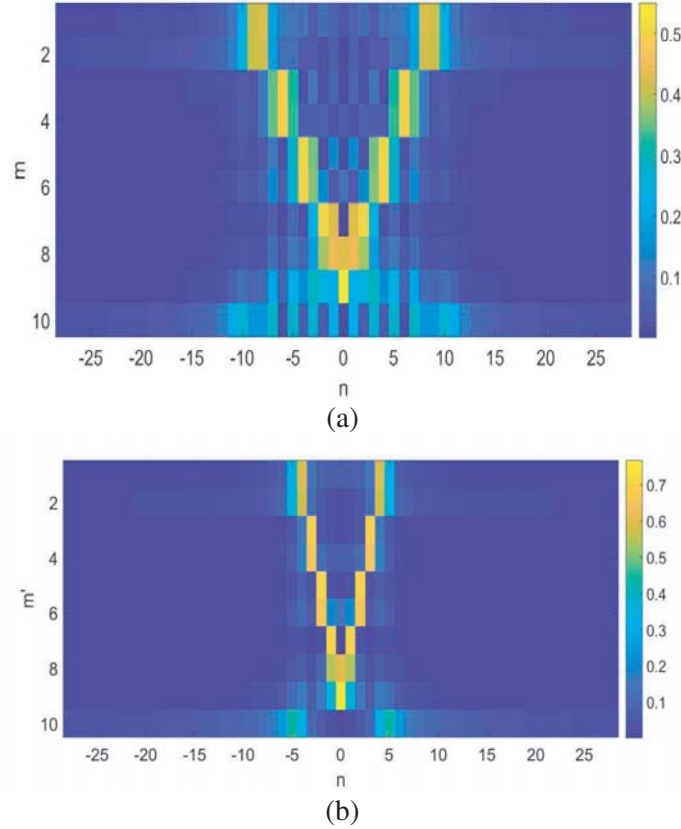


Figure 5. Modulus (a) of the harmonic coefficients v_n^m of the v_n singular functions and (b) of the harmonic coefficients $u_n^{m'}$ of the u_n singular functions, for the geometry of Fig. 4.

Instead, when either α or γ is equal to π , the NDF is very well approximated by either $2M + 1$ or $2M' + 1$. Fig. 6 shows the behavior of the SVs versus the index n normalized to $2M + 1$. As can be seen, in all cases the NDF is very well estimated by $2M + 1$, since the knee appears always at $n \cong 2M + 1$. Moreover, the behavior of the SVs before the knee is not flat, but it exhibits some kind of dynamic. This means that, as discussed in Section 2.2, in the presence of a high level of uncertainties on data, stability requirements can drastically reduce the class of source currents that can be reconstructed.

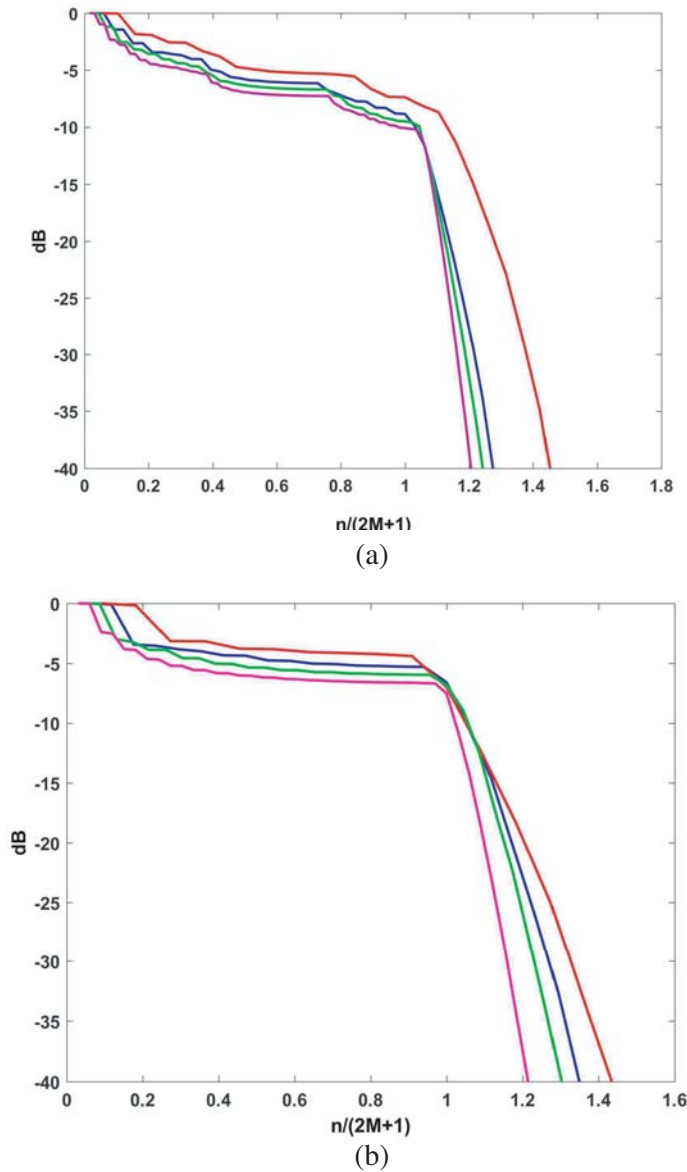


Figure 6. Normalized behavior of the SVs vs their index normalized to $2M + 1$ for circumference arc sources $\gamma = \pi$. (a) $\alpha = \pi/2$, (b) $\alpha = \pi/4$, for $a = 5\lambda$ (blue line), 3λ (red line), 7λ (green line), 10λ (purple line).

2.5. Linear Source

For a $2l$ long linear source aligned along the y axis (see Fig. 7 for the geometry) in Eq. (1) becomes

$$\mathcal{L}(J) = \int_{-l}^l J(y) e^{j\beta y \sin \theta} dy \quad (10)$$

When $OD = [-\pi, \pi]$ some insight about the singular values can be derived by examining the harmonic content of the radiated field. In fact, by applying the Bessel-Anger expansion to the exponential kernel in Eq. (10), it can be shown that only $2N + 1$ Fourier coefficients, with $N \cong [\beta a]$, are significant, after they decay exponentially. However, this result provides an exceedingly upper bound for the NDF.

The discussion in Section 2.4 makes it possible to achieve a stricter estimation for it. In fact, the $2l$ long linear source can be viewed as a chord of a circumference of radius $a = l/\sin \alpha$. As the angle

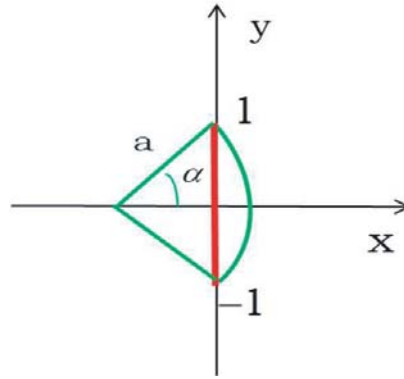


Figure 7. Geometry of a circumference source.

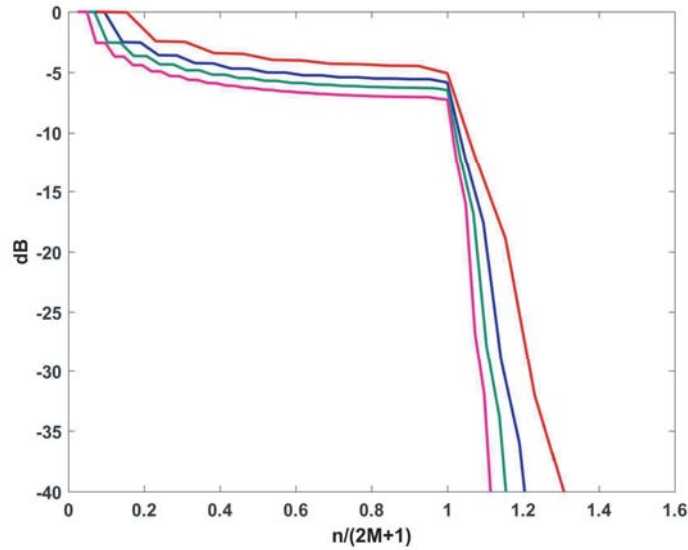


Figure 8. Normalized behavior of the SVs of a linear source vs. their index normalized to $2M + 1$ for $a = 5\lambda$ (blue line), 3λ (red line), 7λ (green line), 10λ (purple line).

α approaches zero (see Fig. 7), the latter can be blended into the subtended arc. Therefore, in virtue of the discussion in the previous section, $M = \eta\beta a\alpha/\pi \approx \eta\beta l/\pi(\alpha/\sin\alpha) \rightarrow [2l\eta/\lambda]$ as $\alpha \rightarrow 0$ and the NDF is $2M + 1$ at most. In particular, when $\gamma \leq \pi/2$, $\eta = \sin(\gamma)$ and $2M + 1 = [4l \sin(\gamma)/\lambda] + 1$.

This expectation is confirmed by the numerical SVD of Eq. (10). In particular, in Fig. 8 the SVs are shown for different values of l . It can be appreciated that our prediction works very well.

The results of the previous Section about the singular functions for an arc source allow to forecast the general behavior of both the u_n and v_n functions in terms of their harmonic content, so that a similar ‘passband’ behavior can be expected with more rapidly varying functions in correspondence to the highest SVs.

A converging estimate of the NDF can be obtained by introducing the spectral variable $w = \sin\theta$, so that the relevant operator can be written as

$$\hat{\mathcal{L}}(J) = \int_{-l}^l J(y) e^{j\beta y w} dy = F(w) \quad (11)$$

where $w \in [-\sin\gamma, \sin\gamma]$. Now, the SVD of Eq. (11) is known [14] in terms of the so called prolate spheroidal wave functions. An important result of [15] concerns the behavior of the σ_n SVs, which are

nearly constant for $n < 2M + 1$ where $M = \lceil \beta \sin \gamma l / \pi \rceil = \lceil 2 \sin \gamma l / \lambda \rceil$, before the typical exponential decay. Unfortunately, the singular values of the operator $\hat{\mathcal{L}}$ are not equal to those of \mathcal{L} ; however, this number is in agreement with the above result concerning the operator in Eq. (10), despite the nonlinear but monotonic change of variable. Accordingly, this suggests that the use of either θ or $w = \sin \theta$ does not affect the NDF, but rather it provides a shaping of the singular value behavior.

3. POINT SPREAD FUNCTION ANALYSIS

In order to appreciate the impact of the source geometry and the limited observation domain on the resolution, a PSF analysis is performed. The PSF is defined as

$$\text{PSF}(\phi, \phi_0) = \sum_{i=0}^{\text{NDF}} v_i(\phi) v_i^*(\phi_0) \tag{12}$$

where ϕ_0 is the location of the impulsive source.

First, we consider the case of a circumference source ($\alpha = \pi$) and full angle observation domain ($\gamma = \pi$). Then a closed form of the PSF can be derived as $\text{PSF}(\phi, \phi_0) = \frac{\sin[\frac{2N+1}{2}(\phi-\phi_0)]}{2\pi \sin(\frac{\phi-\phi_0}{2})}$, which reveals that the resolution, related to the width of the main lobe of the PSF function, is independent on ϕ_0 . For instance with $a = 3\lambda$ and $N = 19$, it is approximately equal to $2 \cdot 2\pi / (2N + 1) \approx 2 \cdot 9.2^\circ$.

When the operator \mathcal{L} is provided by Eq. (4), an expression for the PSF cannot be derived in closed form. However, some information about it can be obtained by considering the operator $\mathcal{L}^\dagger \mathcal{L}$ provided by

$$\mathcal{L}^\dagger \mathcal{L}(J) = \int_{-\alpha}^{\alpha} J(\varphi') \int_{-\gamma}^{\gamma} e^{2j\beta a \sin[\theta - (\phi + \phi')/2] \sin[(\phi - \phi')/2]} d\theta a d\phi'$$

When $\gamma = \pi$, the kernel function of $\mathcal{L}^\dagger \mathcal{L}$ is equal to $2\pi J_0[2\beta a \sin[(\phi - \phi')/2]]$, and, hence, it is convolutional. This makes the PSF spatially invariant resulting in a spatially invariant resolution.

On the contrary, when $\gamma < \pi$ this is not true anymore, and the resolution becomes dependent on ϕ_0 .

The expectations are confirmed by the numerical examples shown in Figs. 9 and 10. The first one reports the PSF for $\alpha = \pi/2$ and $\gamma = \pi$, and for different ϕ_0 . Here, it can be appreciated how the resolution remains unchanged as ϕ_0 varies.

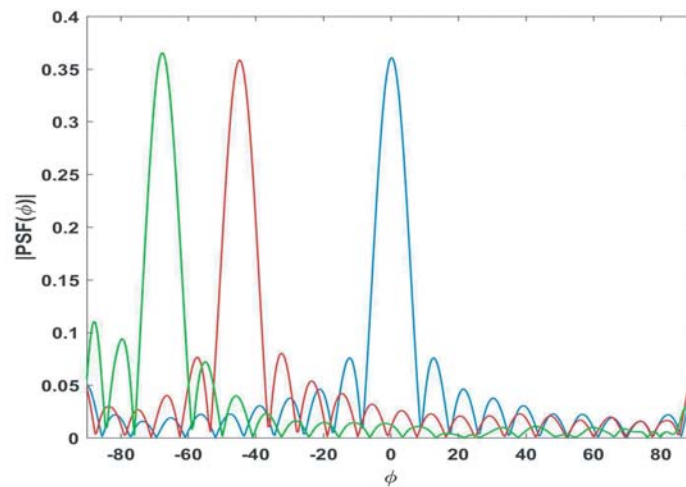


Figure 9. Behavior of the PSF function for a half circumference source ($a = 3\lambda$) for $\alpha = \pi/2$ and $\gamma = \pi$ when centered at $\phi_0 = 0$ (blue line), $\phi_0 = -\pi/4$ (red line), $\phi_0 = -3\pi/8$ (green line).

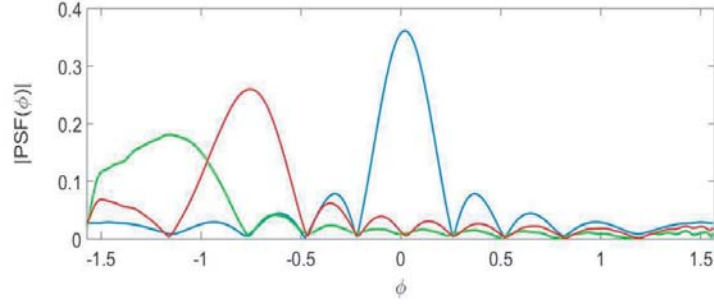


Figure 10. Behavior of the PSF function for an half circumference source ($a = 3\lambda$) for $\alpha = \pi/2$ and $\gamma = \pi/4$ when centered at $\phi_0 = 0$ (blue line), $\phi_0 = -\pi/4$ (red line), $\phi_0 = -3\pi/8$ (green line).

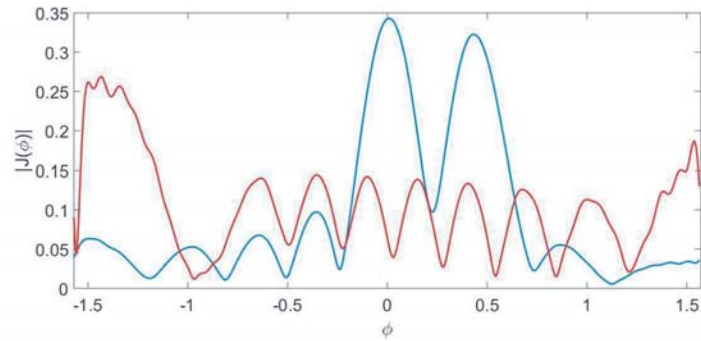


Figure 11. Reconstruction of two point-like sources spaced at $\Delta\phi = 0.42$ and centered at $\phi_0 = 0.2$ (blue line) and $\phi_0 = -1.05$ rad (red line), respectively.

In Fig. 10, the PSF for $\gamma = \pi/4$ is shown for different ϕ_0 . As can be seen, the resolution is not constant and degrades as ϕ_0 moves away from 0° . In particular, for $\phi_0 = 0^\circ$ the main lobe width of the PSF function is very close to the minimum one. On the contrary, the main lobe width enlarges and nearly doubles when ϕ_0 moves towards $\pi/2$.

Accordingly, it can be concluded that the reduction of the observation angle entails the important consequence that source reconstruction is not possible with the same resolution over the whole source support.

The practical relevance of a spatially variant resolution can be appreciated when it is required to reconstruct two point-like sources, as for instance in a radio localization application. Then Fig. 11 shows clearly that, due to the limited observation domain, two equally spaced sources cannot be detected and identified if they are located towards the edge of the half-circumference source domain.

4. EFFECT OF THE SVD ON SOURCE IMAGING AND DIAGNOSTICS

4.1. Imaging of a Circumference Source

The practical relevance of discussions of the previous Section can be shown numerically by referring to a circumference source. As an example of an inverse source problem, we consider the reconstruction of two currents: a rectangular window source, i.e., $J(\phi) = \Pi(\phi/\pi)$, and one radiating a high directivity, single main lobe far field pattern, with $J(\phi) = e^{-J\beta a \cos \phi}$ and $E(\theta) = 2\pi a J_0(2\beta a \sin(\theta/2))$. Thus, the first one mimics a problem where it is required to identify the source location over a circumference and its angular extension from far zone data, while the second one can be of interest in an antenna diagnostics application. Therefore, the corresponding radiation patterns are also displayed. Far zone data are assumed to be collected over a sufficiently high number of samples over a full angle domain.

Different reconstructions are considered at different truncation levels of the TSVD, corresponding to different uncertainty levels. This implies that a different number of singular functions is retained in the reconstruction.

Source reconstructions of Figs. 12 and 13 confirm the expectations about the ‘band-pass’ behavior

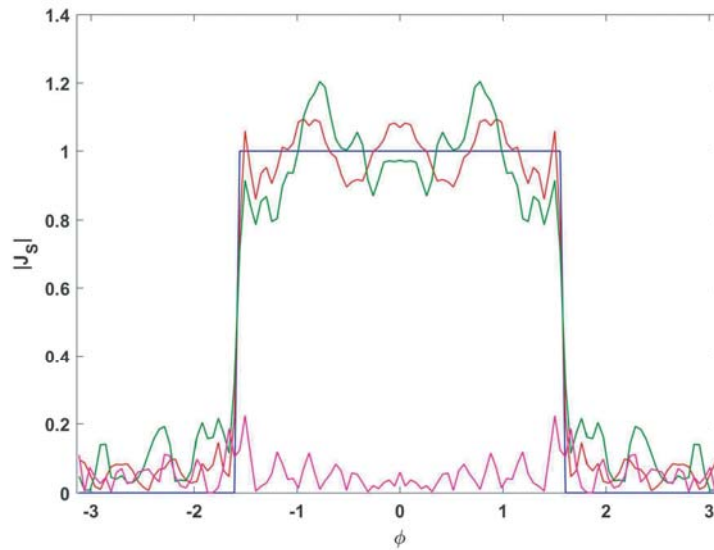


Figure 12. Reconstruction of a constant current source for $|\varphi| < \pi$ (blue line) on a circumference of radius $a = 5\lambda$ by the TSVD algorithm with truncation level at -20 dB (67 SVs, red line), -10 dB (51 SVs, green line), -5 dB (30 SVs, purple line).

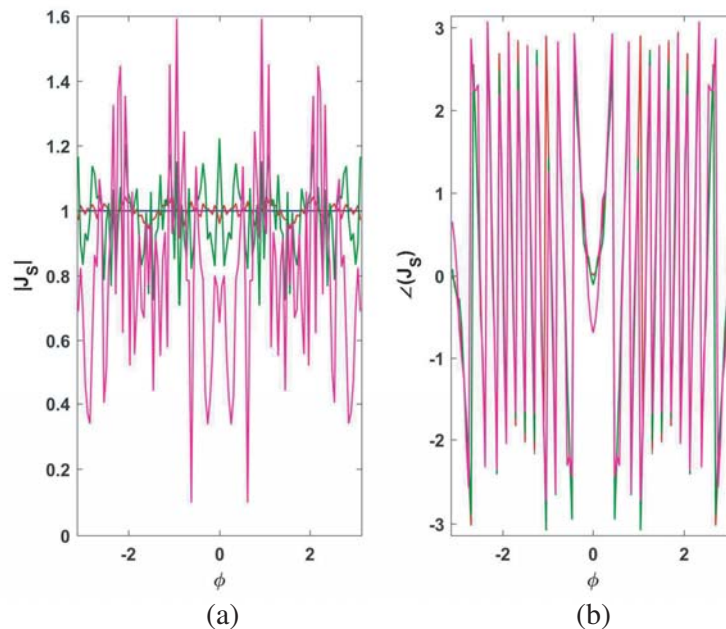


Figure 13. Reconstruction of (a) the modulus and (b) phase of the current (blue line) of a circumference source of radius $a = 5\lambda$ corresponding to a focusing beam by the TSVD algorithm with truncation level at -20 dB (67 SVs, red line), -10 dB (51 SVs, green line), -5 dB (30 SVs, purple line).

of the radiation operator. In fact, when the filtering over the SV is greater, i.e., when the threshold is -5 dB, the reconstruction of the source is affected by large error (see the purple line in Fig. 13) or cannot be carried out at all (see the purple line in Fig. 12). This fact is related to the harmonic content of the source, since the ‘window’ source has mainly a low order harmonic content, which is filtered out by the “bandpass” behavior of the regularizing imaging algorithm. Moreover, the radiation patterns corresponding to the reconstructed source currents (shown in Fig. 14) can provide completely inaccurate pieces of information, for instance about the side lobe envelope behavior.

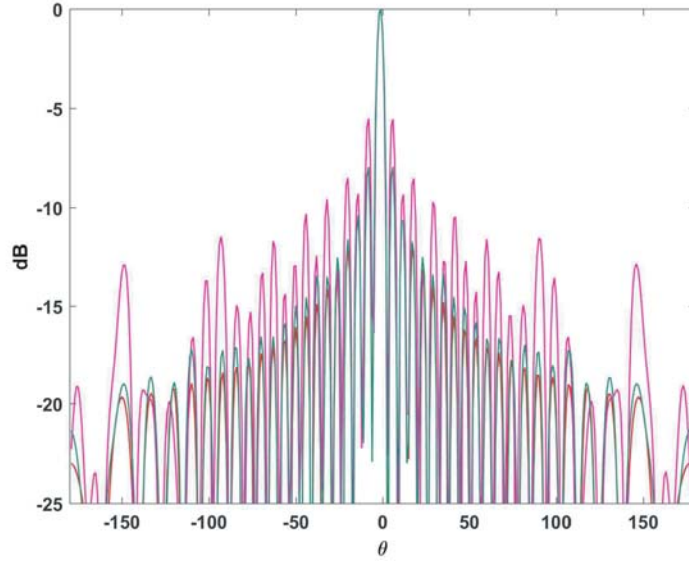


Figure 14. Reconstruction of the far field $E(\theta)$ function of the current corresponding to the currents of Fig. 4 obtained by different TSVD truncation level (the exact result by blue line is indistinguishable from the reconstruction by red line with truncation at -20 dB).

4.2. Application to Array Diagnostics

Another practical important application of the NDF estimation and the PSF analysis can be fully appreciated when we consider a problem of array diagnostics for fault detection and apply the TSVD algorithm truncating the SVs to the NDF.

As an example, we consider an array of 9 isotropic line sources located over an arc of a circumference with radius $a = 3\lambda$ and radiating a focusing beam towards the direction $\theta_0 = 0^\circ$, so that the source coefficients follow the typical $c_i = e^{-j\beta a \cos(i\Delta\phi)}$ law, with $i = -4, \dots, 4$ and $\Delta\phi = \pi/9$. The observation domain in far zone is restricted to $\gamma = \pi/4$. We suppose that two nonconsecutive array elements may be off. By referring to the SVs behavior depicted in Fig. 4, the actual NDF is appreciated as high as 10. Accordingly, we expect to be able to reconstruct reliably a discrete source with the same (or a lower) number of elements. This is confirmed by the results of Fig. 15, where the modulus of the reconstructed current is shown, and an array element is supposed to be off when the reconstructed current at its location is lower than 0.5.

As a further example, we consider an array with 15 isotropic elements located on the same half circumference as above with $\Delta\phi = \pi/15$ so that the array elements are spaced at about $\Delta s = a\Delta\phi \approx 0.6\lambda$. The comparison of the reconstructions of the modulus of the array coefficients is shown again for off elements located at the edge of the array (Fig. 16) for the same partial observation domain ($\gamma = \pi/4$). It can be appreciated how the results can become unsatisfactory because both the NDFs are lower than the number of array elements, and the PSF is not spatially invariant. Then it is clear that the width of the observation domain must be carefully taken into account in array diagnostics.

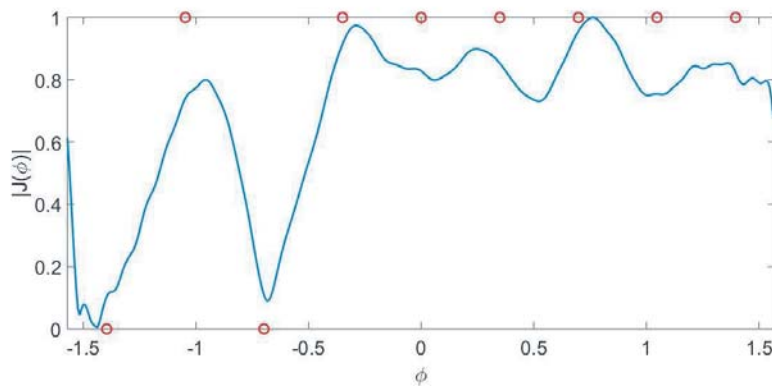


Figure 15. Reconstruction of the modulus of the source current corresponding to a 9 elements array of isotropic linear sources located over a half circumference ($a = 3\lambda$) when $\gamma = \pi/4$. Red circles reports the actual modulus of each array element.

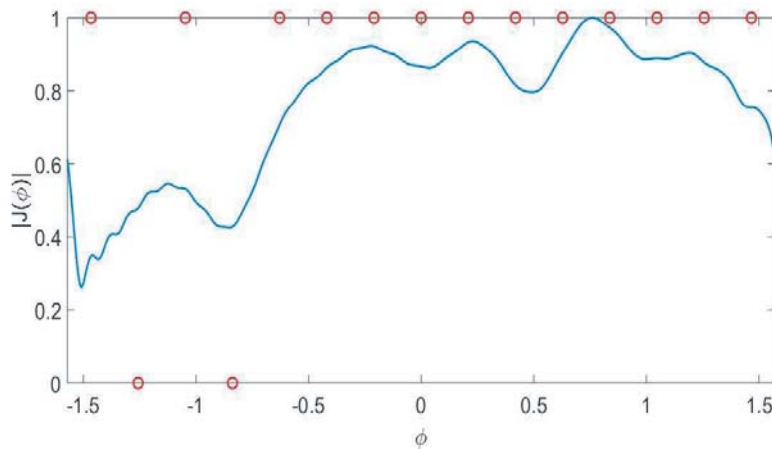


Figure 16. Reconstruction of the modulus of the source current corresponding to a 15 elements array of isotropic linear sources located over a half circumference ($a = 3\lambda$) when $\gamma = \pi/4$. Red circles reports the actual modulus of each array element.

5. CONCLUSIONS

The influence of the source geometry and of the width of the observation domain on the spectral decomposition of the radiation operator has been examined for some 2D shaped geometries. When the closed form SVD is not available, an appreciation of its features has been gained by a Fourier analysis of both source and radiated field sets. The theoretical results have allowed to evaluate the NDF (or an upper bound about it) and the harmonic content of the singular functions for different geometries.

In addition, the role of the PSF for the analysis of the resolution achievable in inverse source problem is examined. The analysis reveals that the resolution is spatially variant for a limited observation domain. These results imply that source reconstruction is not possible all over the circumference with the same accuracy.

The above arguments provide valuable practical information about the maximum number of source elements that can be reconstructed and about the detection of two close point-like sources. Finally, numerical examples concerning both source reconstructions and array diagnostics are shown. Further potential applications concern the synthesis of conformal antennas. The extension to array antennas [16] and general 3D sources [17] is under development.

REFERENCES

1. Leone, G., "Source geometry optimization for hemispherical radiation pattern coverage," *IEEE Transactions on Antennas and Propagation*, Vol. 64, No. 5, 2033–2038, May 2016.
2. Li, W. T., X. W. Shi, Y. Q. Hei, S. F. Liu, and J. Zhu, "A hybrid optimization algorithm and its application for conformal array pattern synthesis," *IEEE Transactions on Antennas and Propagation*, Vol. 58, No. 10, 3401–3406, 2010.
3. Persson, K., M. Gustafsson, G. Kristensson, and B. Widenberg, "Source reconstruction by far-field data for imaging of defects in frequency selective radomes," *IEEE Antennas Wirel. Propag. Lett.*, Vol. 12, 480–483, 2013.
4. Di Francia, G. T., "Degrees of freedom of an image," *Journal of the Optical Society of America*, Vol. 59, 799–804, 1969.
5. Newsam, G. and R. Barakat, "Essential dimension as a well-defined number of degrees of freedom of finite-convolution operators appearing in optics," *Journal of the Optical Society of America*, Vol. 2, 2040–2045, 1985.
6. Riesz, F. and B. Nagy, *Functional Analysis*, Dover, 1990.
7. Bertero, M. and P. Boccacci, *Introduction to Inverse Problems in Imaging*, IOP Publishing, 1998.
8. Solimene, R., M. A. Maisto, and R. Pierri, "Inverse source in the presence of a reflecting plane for the strip case," *Journal of the Optical Society of America A*, Vol. 31, No. 12, 2814–2820, 2014.
9. Solimene, R., M. A. Maisto, and R. Pierri, "Role of diversity on the singular values of linear scattering operators: The case of strip objects," *Journal of the Optical Society of America A*, Vol. 30, No. 11, 2266–2272, 2013.
10. Solimene, R., M. A. Maisto, G. Romeo, and R. Pierri, "On the singular spectrum of the radiation operator for multiple and extended observation domains," *International Journal of Antennas and Propagation*, <http://dx.doi.org/10.1155/2013/585238>, 2013.
11. Solimene, R., M. A. Maisto, and R. Pierri, "Inverse scattering in the presence of a reflecting plane," *Journal of Optics*, Vol. 18, No. 2, 025603, 2015.
12. Leone, G., M. A. Maisto, and R. Pierri, "Application of inverse source reconstruction to conformal antennas synthesis," *IEEE Transactions on Antennas and Propagation*, Vol. 66, No. 3, 1436–1445, Mar. 2018.
13. Solimene, R. and R. Pierri, "Number of degrees of freedom of the radiated field over multiple bounded domain," *Optics Letters*, Vol. 32, No. 21, 3113–3115, 2007.
14. Slepian, D. and H. O. Pollack, "Prolate spheroidal wave functions, Fourier analysis, and uncertainty — I," *Bell Syst. Techn. J.*, Vol. 40, 43–63, 1961.
15. Landau, H. J. and H. O. Pollack, "The eigenvalue distribution of time and frequency limiting," *J. Math. Phys.*, Vol. 77, 469–481, 1980.
16. Leone, G., M. A. Maisto, and R. Pierri, "Inverse source reconstruction for the synthesis on conformal domains," *2017 International Conference on Electromagnetics in Advanced Applications (ICEAA)*, Verona, Italy, Sep. 2017.
17. Leone, G., M. A. Maisto, and R. Pierri, "First step towards a comparison between 3D source geometries for conformal antennas," *12th European Conference on Antennas and Propagation (EUCAP 2018)*, London, UK, Apr. 2018.